CFD Lagrangian Modeling of Water Droplet Transport for ISS Hygiene Activity Application

Chang H. Son[1]
The Boeing Company, Houston, TX, 77059, United States

The goal of this study was to assess the impacts of free water propagation in the Waste and Hygiene Compartment (WHC) installed in Node 3. Free water can be generated inside the WHC in small quantities due to crew hygiene activity. To mitigate potential impact of free water in Node 3 cabin the WHC doorway is enclosed by a waterproof bump-out, Kabin, with openings at the top and bottom. At the overhead side of the rack, there is a screen that prevents large drops of water from exiting. However, as the avionics fan in the WHC causes airflow toward the deck side of the rack, small quantities of free water may exit at the bottom of the Kabin. A Computational Fluid Dynamics (CFD) analysis of Node 3 cabin airflow enable identifying the paths of water transport. To simulate the droplet transport the Lagrangian discrete phase approach was used. Various initial droplet distributions were considered in the study. The droplet diameter was varied in the range of 5-20 mm. The results of the computations showed that most of the drops fall to the rack surface not far from the WHC curtain.

I. Introduction

THE International Space Station (ISS) ventilation system performance is an important factor for on-board crew support. Each Environmental Control and Life Support System (ECLSS) zone should be tested from the ventilation effectiveness point of view and consequently the crew safety perspective. Special attention should be paid to the Waste and Hygiene Compartment (WHC) ventilation because the compartment is supplied with the privacy protection bump-outs, Kabin, that separate WHC from the cabin and prevent airflow in the WHC. To force air circulation inside WHC and to intensify air exchange between the compartment and the cabin, an avionics fan discharge and intake are placed inside the WHC. The WHC is installed in the Node 3 module berthed to the port side of Node 1. Assessment of the overall ventilation characteristics of the Node 3 cabin and WHC interior was performed earlier.[1,2]

The crew hygiene activities in the WHC could lead to free water propagation due to hand movement of crew cleaning their head and body. The WHC doorway is enclosed by a waterproof curtain with openings at the top and bottom. To protect the cabin from free water the WHC is supplied with the top covering grid that prevents large drops of water from exiting. However, as the avionics fan in the WHC causes airflow toward the deck side of the rack, small quantities of free water may exit at the bottom of the Kabin.

The goal of the study is to identify the water transport path and to estimate the probability of the droplet transport to the adjacent rack surface with electronic equipment. Numerical modeling has been performed with the Computational Fluid Dynamics (CFD) technique using the ANSYS FLUENT 12.1.4 CFD software.[2]

II. Computational Model

A. Cabin Aisle Way Geometry Model and Airflow Boundary Conditions

The geometry model adopted for the CFD analysis of the Node 3 cabin air ventilation is shown in Fig. 1. The computational domain included the WHC and Advanced Resistive Exercise Device (ARED) protrusions into ECLS keep-out zones. A crew-member model, ECLOID (ECLSS AndrOID) was incorporated into the WHC cabin. The total volume of the Node 3 cabin aisle way considered in the present CFD analysis of the cabin ventilation is 33 m^3.

The Node 3 common air supply diffusers are placed in the rack bay in corner pockets stretched in the longitudinal direction (in the port-starboard direction). Each Node 3 aft-side cabin air supply diffusers (#CD1 and

[1] ISS ECLSS Analysis Lead, 13100 Space Center Blvd, e-mail: chang.h.son@boeing.com.

#CD2 in Fig. 1) has a given total flow rate of 60 cfm that corresponds to the total supply flow rate of 120 cfm. Each Node 3 forward-side cabin air supply diffuser (#CD3 and #CD4 in Fig. 1) has a given total flow rate of 80 cfm that corresponds to the total supply flow rate of 160 cfm. The aft-side supply diffusers direct the airflow across the ceiling of the rack bay (in the direction from aft to forward), while the forward-side supply diffusers direct the airflow towards the deck. So, the global circulation loop is formed in the rack bay of the Node. Note also that the flow from each diffuser is divided into two parts in the aft-forward direction, with the flow angles of 60° and –60° respectively. The velocity inlet boundary condition is set for each half of each diffuser with the velocity specification method of velocity magnitude and flow direction components. The uniform inlet velocity approximation is assumed on the velocity inlet boundaries.

The Node 3 linear diffusers are arranged in the radial bay (#LD1 and #LD2 in Fig. 1). Each linear diffuser has a given total flow rate of 120 cfm that corresponds to the total supply flow rate of 240 cfm. The velocity inlet boundary condition is set for each diffuser with the velocity specification method of velocity magnitude normal to the boundary.

Two Node 3 return grilles are placed in the rack bay, at the deck (#RG1 and #RG2 in Fig. 1). The velocity inlet boundary condition are set for the return grilles (outlets for the flow domain analyzed). The total flow rate leaving the Node 1 module through each return grille is 260 cfm that corresponds to the total supply flow rate of 520 cfm.

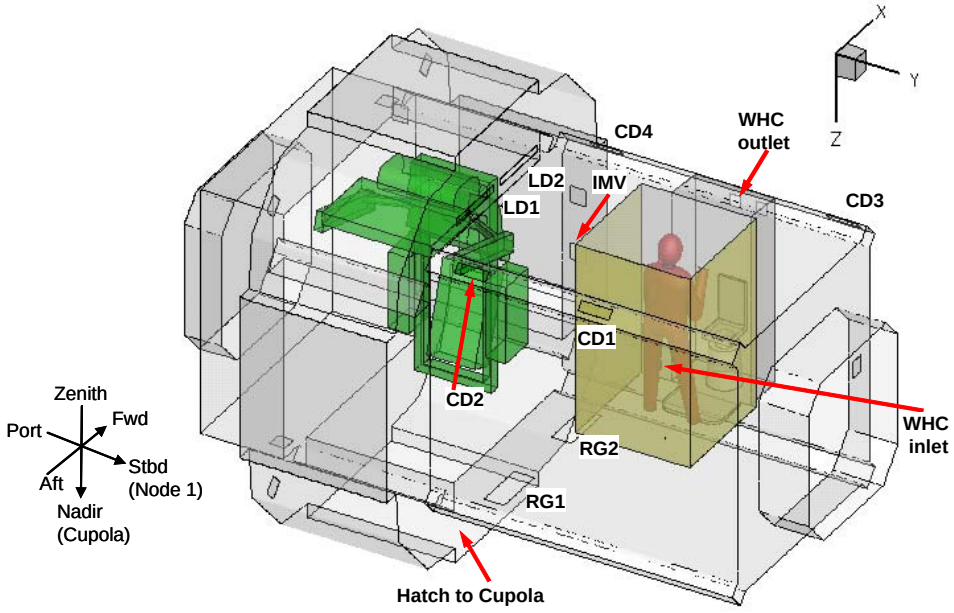

Figure 1. Node 3 geometry model and notation of boundaries.

The forward Inter-module Ventilation (IMV) Node 3 diffuser is open (the lower one, #IMV in Fig. 1), it supplies IMV air to the Cupola module attached to the Node 3 nadir hatch. The flow rate leaving the Node 3 cabin through the IMV diffuser is 120 cfm. The velocity inlet boundary condition is set for the boundary (an outlet for the flow domain analyzed). IMV air (120 cfm) returns from Cupola to the Node 3 cabin through the open hatch.

To organize air circulation inside WHC and to intensify air exchange between the compartment and the cabin, avionics fan discharge and intake are placed inside the WHC. The WHC intake/discharge configuration corresponds to the WHC flow rate of 40 cfm and the port WHC outlet is active. The WHC inlet is placed in the bottom of the back WHC wall.

The mesh closing WHC from the top (zenith) is a permeable body with an open area of 37%. A porous jump model is used to simulate the closing mesh effect on the airflow. The porous jump conditions are used in ANSYS FLUENT to model a thin "membrane"' that has known velocity (pressure-drop) characteristics. It is essentially a 1D simplification of the porous media model available for cell zones.

The thin porous medium has a finite thickness over which the pressure change is defined as a combination of Darcy's Law and an additional inertial loss term:

$$\Delta p_{visc} = -\left(\frac{\mu}{\alpha} v + C_2 \frac{1}{2} \rho v^2\right) H_{layer} \qquad (1)$$

where μ is the dynamic fluid viscosity, α is the permeability of the medium, C_2 is the pressure-jump coefficient, v is the velocity normal to the porous face, and H_{layer} is the thickness of the medium. The pressure losses due to the viscous term (Darcy's Law, the first item in Eq. 1) are neglected setting a high value of α (say, $\alpha = 1\times10^{10}$). The inertial term is proportional to the dynamic head with the coefficient $C_2 = 4.3$. The pressure loss coefficient estimation is based on the data resistance of a steel-wire mesh in the cross-flow given in Ref. 4.

The no-slip boundary condition is imposed on all of the solid surfaces. The air is assumed to be an incompressible fluid. The properties of the fluid are as follows: density of $\rho = 0.0765$ lbm/ft^3, and dynamic viscosity of $\mu = 1.202\times10^{-5}$ lbm/ft·s.

B. Water Droplet Transport Problem Formulation

This analysis assesses impacts of free water exiting the WHC. The assumed volume of each droplet is in the range from 0.06 ml to 5 ml that corresponds to the droplet diameter in the range from 0.2" to 0.8" (5-20 mm). To simulate the droplet transport, the Lagrangian discrete phase approach was used, and the droplet transport was computed in the given steady-state air velocity field. The zero initial droplet velocities were set as the initial conditions for the main runs. To investigate the effect of the initial conditions, a special run with the initial droplet velocity of 5 ft/min was computed. In all the cases the "escape" condition was assumed on all the walls, so that the droplet collapses if it reaches the wall.

Two different droplet injection scenarios were considered. For the first droplet injection scenario, the problem settings were as follows. The uniform distribution of the droplets of given size were set at the gap surfaces (a so called surface distribution), and their transport was computed in the given air velocity field.

For the second droplet injection scenario, the uniform distribution of droplets was set within the WHC cabin at a plane slice located at 3/4 high up towards overhead side. This is about the height of the crew head cleaning their hair. This task estimated how many droplets penetrate to the Node 3 cabin, and how many droplets remain at the walls of the WHC curtain and go to the WHC intake.

C. Computational Aspects and Turbulence Modeling

The computational grid generated for the CFD modeling of Node 3 ventilation is fully unstructured with tetrahedral mesh elements. The tetrahedral grids were created using the GAMBIT 2.4.6 generator.[8] The grid is clustered to the solid walls and to the diffusers.

The FLUENT solver, being face-based, supports polyhedral cells.[5] The advantages that polyhedral meshes have shown over some of the tetrahedral or hybrid meshes is the lower overall cell count, almost 3-5 times lower for unstructured meshes than the original cell count, keeping the same spatial accuracy.

Conversion of the initial tetrahedral grid to polyhedral one was performed in FLUENT, see Ref. 6 for details. The clustering of the grids to the walls and to the diffusers was kept during the conversion procedure. The final polyhedral grid consisted of more than one million cells.

The Reynolds-Averaged Navier-Stokes (URANS) approach was employed. The RANS-based modeling approach greatly reduces the required computational effort and resources, and is widely adopted for practical engineering applications. For the ISS ventilation case, a comparison of the Columbus experimental data with the results of 3D steady-state RANS computations as well as with the accurate Large Eddy Simulation computations prove that RANS modeling is quite accurate regarding to air ventilation velocity field.[9]

The standard k-ε model, with the standard wall functions, was used for computations.[5] For all the cases computed, the wall distance of a cell centre adjacent to a solid wall measured in wall units, y_p^+, ranged from 10 to 50 over the majority of the solid walls. The inlet turbulence intensity was taken as 10% for all the diffusers while the inlet ratio of the turbulent to molecular viscosity, ν_{tur}/ν, was varied from diffuser to diffuser to ensure that the inlet-jet effective Reynolds numbers, $Re_{eff} = V_{in}L_s/(\nu+\nu_{tur})$, are within the range from 200 to 300. Here V_{in} is the inlet velocity value, and L_s is the inlet length scale (the diffuser width).

To obtain an airflow solution, the governing equations for conservation of mass, momentum, and turbulence characteristics were solved using the steady coupled pressure-based solver.[2] The coupled solver was chosen as it provided the best convergence for both the cases considered. The second-order upwind spatial discretization scheme was used, both for the momentum and the k-ε model governing equations. The second-order pressure interpolation scheme was employed. The Courant number of 200 was kept, while the under-relaxation factors of 0.85 were set for the momentum and pressure.

The convergence criteria are as follows. Each computational run was computed untill the residual values are reduced by 5 orders. Additionally, the mass flow rate through the boundaries was controlled, and the mass balance of 10^{-6} has been achieved.

For numerical simulation acceleration, parallel computations were performed using eight processes of a LINUX-based cluster.

III. Results and discussion

Fig. 2 illustrates the global air flow structure in the Node 3 cabin: pathlines issued from the module inlet diffusers are colored with air velocity magnitude. The data for the converged steady-state airflow field is given. As it is visible from Fig. 2g, air penetrates from the WHC interior into the cabin through the gaps between the waterproof curtain and the floor and ceiling. It is noticeable that only few pathlines end at the WHC outlet. It indicates a real possibility of water penetration of water droplets to the cabin.

The effect of the flow through the gaps between the waterproof curtain and the module floor is shown in Fig. 3 for the port gap (the "left" one, at lower *y*-value, see Fig. 1), Fig. 4 for the starboard gap (the "right" one, at higher *y*-value), and Fig. 5 for the aft gap (the gap in front of the curtain, at the constant *x*-value). The initial droplet distributions were evenly spread over uniform meshes of 50 points set at each of three gaps (Fig. 3b, 4b, and 5b), and droplet tracks were computed for three different injections.

The air velocity field at the gaps between the WHC curtains and the deck is shown in Fig. 3a, 4a, and 5a. The normal velocity is given in the plots, and the flow direction is clearly indicated. The regions with "positive" (from the WHC interior to Node 3 cabin) and "negative" (to the WHC interior) flow were registered for each gap. Remarkably that at the "front" gap the flow is directed mainly from the WHC interior to the Node 3 cabin, while at the "right" gap (Fig. 5a) the flow is directed mainly from the Node 3 cabin to the WHC interior. This flow structure is determined by the inlet flow from the common diffusers as it is visible in Fig. 2c, the jet from the diffuser CD3 is directed to the deck and penetrates to the WHC interior through the "right" gap.

The pathlines issued from the gaps are shown in Fig. 3c, 4c, and 5c. The droplet tracks are shown in Fig. 3d, 4d, and 5d. Note that each 4^{th} pathline and droplet track is shown in the plots. The particle tracks differ much from the pathlines as heavy droplets do not follow the air due to inertia. After penetration to the Node 3 cabin the droplets mostly move to the floor and walls not far from the WHC waterproof curtain.

Zero initial velocities were set for the injections presented in Fig. 3, 4, and 5. In fact, the droplets generated inside WHC travel through the WHC cabin, and some of them could be found at the gap surface with some initial velocity. In the current modeling the droplets of zero-velocity are issued from the gap surface, so that their prehistory is neglected. Fig. 6f and 6d illustrate a study of droplet initial velocity influence on the particle tracks. The effect of droplet initial velocity in the range considered is not high.

Fig. 6b and 6c illustrate a study of droplet diameter influence on the particle tracks. The only difference in two runs is that the first one (Fig. 6b) is for the initial droplets of 0.8" diameter corresponding to 5 ml droplets, while the second one (Fig. 6c) is for light droplets of 0.2" diameter that corresponds to the volume of 0.6 ml. The effect of droplet diameter in the range of 5-20 mm is negligible.

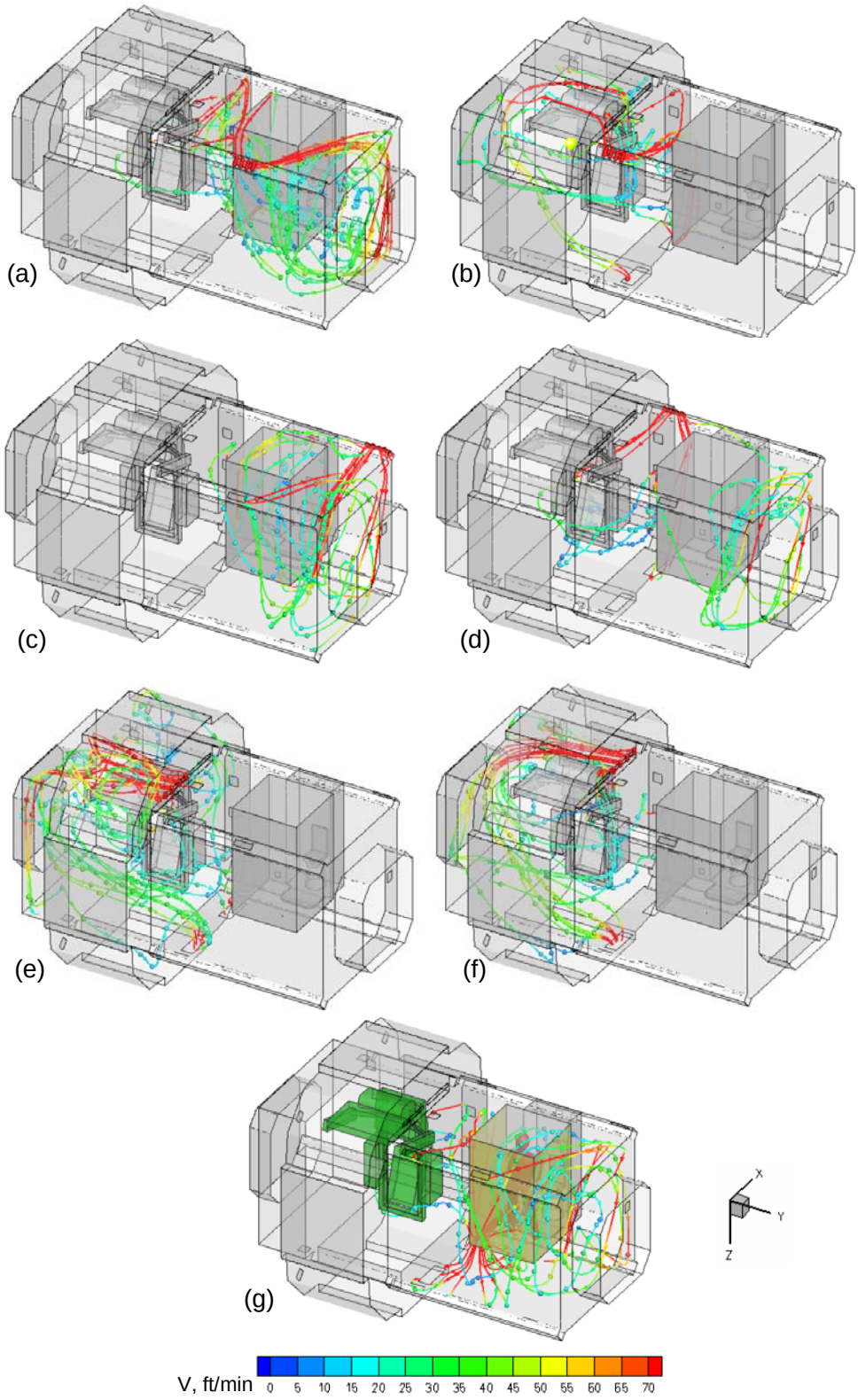

Figure 2. Pathlines colored by velocity magnitude issued from the WHC Cabin Ventilation Diffuser Geometry model for Cygnus and Node 2 cabin ventilation analysis issued from: (a) CD1, (b) CD2, (c) CD3, (d) CD4, (e) LD1, (f) LD2, (g) WHC cabin inlet diffuser.

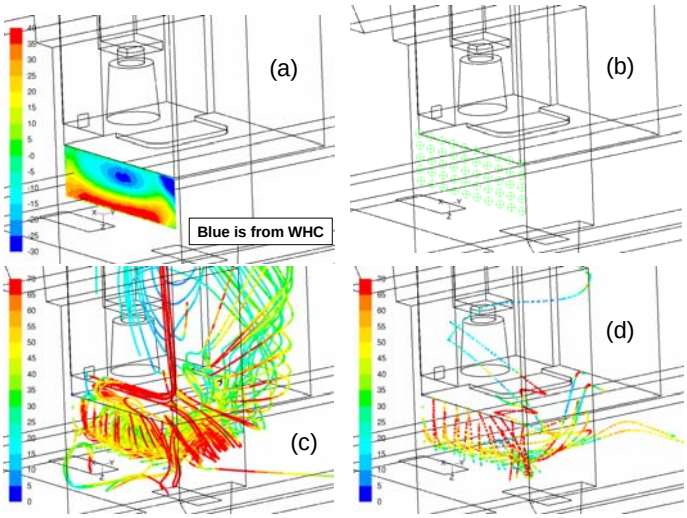

Figure 3. Data for the curtain/floor "left" gap: (a) *y*-velocity field, (b) uniform mesh used for pathlines/tracks issue, (c) pathlines, (d) particle tracks; pathlines/tracks are colored with velocity magnitude.

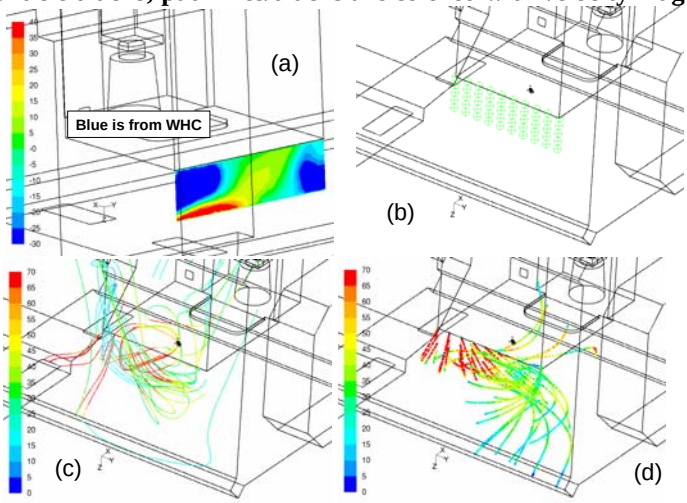

Figure 4. Data for the curtain/floor "front" gap: (a) *x*-velocity field, (b) uniform mesh used for pathlines/tracks issue, (c) pathlines, (d) particle tracks; pathlines/tracks are colored with velocity magnitude.

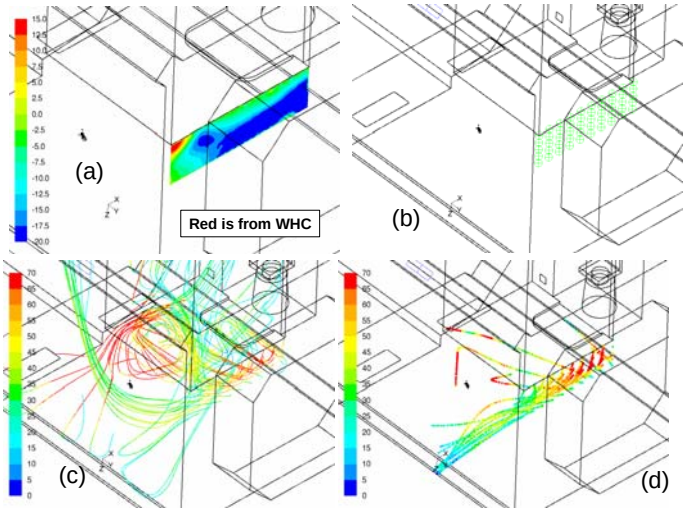

Figure 5. Data for the curtain/floor "right" gap: (a) *y*-velocity field, (b) uniform mesh used for pathlines/tracks issue, (c) pathlines, (d) particle tracks; pathlines/tracks are colored with velocity magnitude.

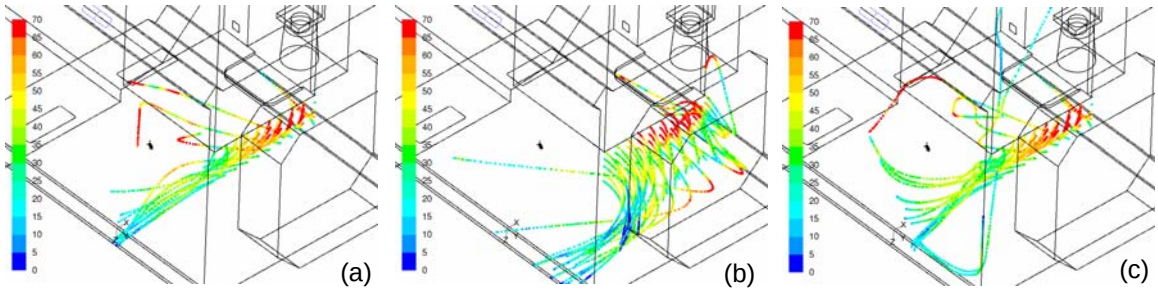

Figure 6. Effect of initial settings of water droplets illustrated for the injection from the "right" gap: (a) zero initial velocity, droplet diameter of 0.8"; (b) same as (a), but initial droplet velocity is 5 ft/min; (c) same as (a), but droplet diameter is 0.2".

We issue droplets from a section inside WHC cabin. The droplets flow with the WHC ventilation air, and partially penetrate to the Node 3 cabin through the top and bottom gaps.

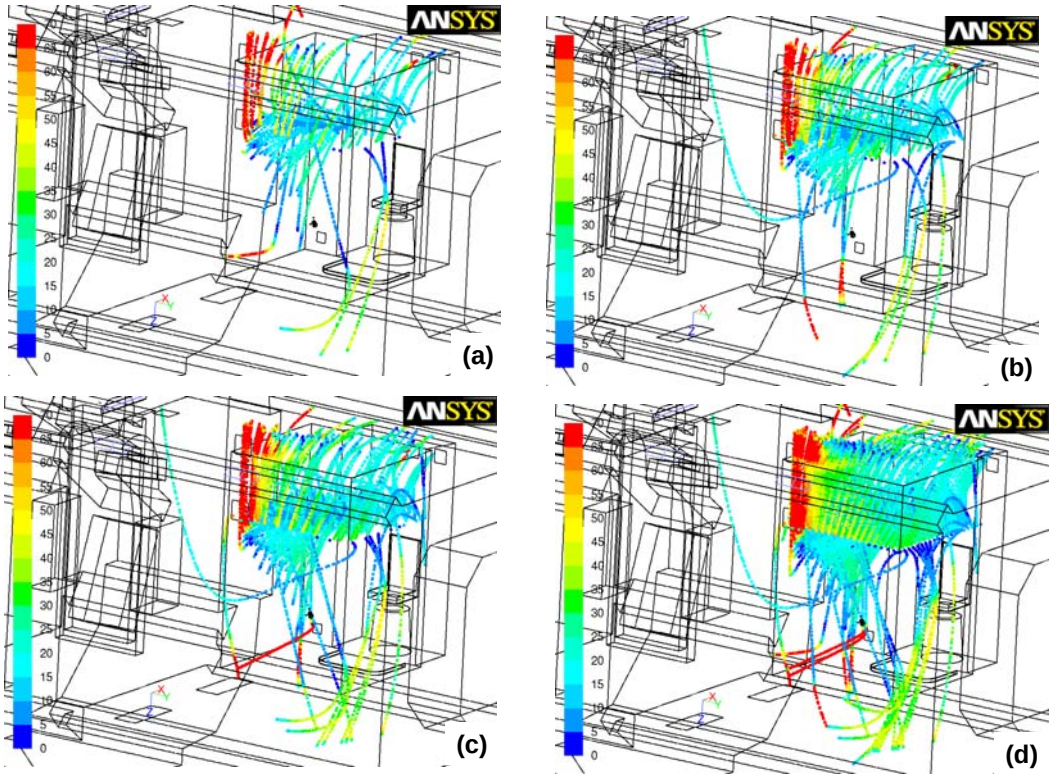

Figure 7. Water drop tracks colored with velocity magnitude issued from the plane section cutting the Node 3 WHC cabin at 3/4 high up toward overhead side. The number of points used for pathlines/tracks issue is varied: (a) 80, (b) 134, (c) 200, (d) 400 points; each 4th pathline/track is shown only; droplet diameter is 0.2".

Fig. 7 shows the droplet tracks that are issued from an interior surface. This surface for free water droplet release is located at 3/4 high up toward overhead side. Four plots shown in the figure present four different cases computed with different number of droplets issued. Using these plots, it is possible to estimate roughly the probability of the droplet transport to the deck surface. As it is visible from Fig. 7, when 80 droplets are issued, 2 or 3 of them reach the deck surface. When 134 droplets are issued, 4-5 tracks reach the deck. When the amount of droplets is increased up to 200, 7-8 of them reach the deck. Finally, among 400 issued droplets about 12-15 reach the deck. As a conclusion, the droplet transport to the adjacent rack surface with electronic equipment is about 4%. It could be concluded that the probability of the droplet transport to the deck surface was estimated as less than 5%.

IV. Conclusion

ISS ventilation characteristics for the Node 3 module with the WHC installed were numerically predicted using the CFD software FLUENT 12.1. The airflow patterns and water droplet tracks in the cabin aisle way were computed to provide a detailed analysis of free water transport. To simulate the droplet transport the Lagrangian discrete phase approach was used. To set the initial conditions, the droplets were distributed (1) over the surfaces of the gaps between the WHC waterproof curtain and the deck and (2) a cross-section of the WHC interior. The results of the computations showed that the droplets do not penetrate far from the bottom WHC-deck gap. Most of the air at the gap surface located near the neighboring rack goes to WHC from the Node 3 cabin that prevents droplet transport in the rack direction. On the other hand, the droplets were very inertial and after penetration to the Node 3 cabin move to the floor and walls not far from the WHC waterproof curtain. It was shown that the effect of droplet diameter in the range of 5-20 mm was negligible. The probability of the droplet transport to the deck surface was estimated as less than 5%.

References

[1] Son, C.H., Smirnov, E.M., Ivanov, N.G., and Telnov, D.S., "Computational Fluid Dynamics Analysis for the Waste and Hygiene Compartment in the International Space Station," *SAE International Journal of Aerospace*, 2009, Vol. 1, No 1, pp 247-253.

[2]Son, C.H., Smirnov, E.M., Ivanov, N.G., and Telnov, D.S., "International Space Station Node 3 CFD Ventilation Modeling for Early Ingress and Nominal Operation," AIAA 2010-6170, AIAA, 2010. 10 p.

[3]ANSYS FLUENT 12.0 Theory Guide. Release 12.0. ANSYS, Inc. January 2009.

[4]Idelchik, I.E., *Handbook of Hydraulic Resistance*, Begell House, 2008.

[5]GAMBIT 2.4 Modeling Guide, Fluent Inc., 2007.

[6]Smirnov, E.M., Ivanov, N.G., Telnov, D.S., and Son, C.H., "CFD modeling of cabin air ventilation in the International Space Station: a comparison of RANS and LES data with test measurements for the Columbus Module," *Int. J. of Ventilation*, Vol. 5, No 2, 2006, pp. 219-228.

[7]Launder, B.E., and Spalding D.B., "The numerical computation of turbulent flows," *Computer Methods in Applied Mechanics and Engineering*, Vol. 3, 1974, pp. 269-289.